Mon. Not. R. Astron. Soc. **000**, 1 - ?? (—) Printed 1 March 2012 (MN LaTeX style file v2.2)

arXiv:1202.3610v2 [astro-ph.CO] 28 Feb 2012

Detectability of High-Redshift Superluminous Supernovae with Upcoming Optical and Near-Infrared Surveys

Masaomi Tanaka[1,2]*, Takashi J. Moriya[2,3,4], Naoki Yoshida[2], and Ken'ichi Nomoto[2]

[1] *National Astronomical Observatory of Japan, Mitaka, Tokyo 181-8588, Japan*
[2] *Institute for the Physics and Mathematics of the Universe, University of Tokyo, Kashiwa, Chiba 277-8583, Japan*
[3] *Department of Astronomy, Graduate School of Science, University of Tokyo, 7-3-1 Hongo, Bunkyo-ku, Tokyo 113-0033, Japan*
[4] *Research Center for the Early Universe, Graduate School of Science, University of Tokyo, 7-3-1 Hongo, Bunkyo-ku, Tokyo 113-0033, Japan*

Accepted —. Received —

ABSTRACT

Observations of high-redshift supernovae (SNe) open a novel opportunity to study the massive star population in the early Universe. We study the detectability of superluminous SNe with upcoming optical and near-infrared (NIR) surveys. Our calculations are based on the cosmic star formation history, the SN occurence rate, the characteristic colour and the light curve of the SNe that are all calibrated by available observations. We show that 15-150 SNe up to $z \sim 4$ will be discovered by the proposed Subaru/Hyper Suprime-Cam deep survey: 30 deg^2 survey with 24.5 AB mag depth in z-band for 3 months. With its ultra-deep layer (3.5 deg^2 with 25.6 AB mag depth in z-band for 4 months), the highest redshift can be extended to $z \sim 5$. We further explore the detectability by upcoming NIR survey utilizing future satellites such as Euclid, WFIRST, and WISH. The wide-field NIR surveys are very efficient to detect high-redshift SNe. With a hypothetical deep NIR survey for 100 deg^2 with 26 AB mag depth at 1-4 μm, at least ~ 50 SNe will be discovered at $z > 3$ in half a year. The number of the detected SNe can place a strong constraint on the stellar initial mass function or its slope especially at the high-mass end. Superluminous SNe at high redshifts can be distinguished from other types of SNe by the long time-scale of their light curves in the observer's frame, the optical colours redder than other core-collapse SNe and the NIR colours redder than any other types of SNe.

Key words: stars: luminosity function, mass function – supernovae: general – early Universe

1 INTRODUCTION

Core-collapse supernovae (SNe) are triggered by massive stars at the end of their lives. Thanks to the high luminosity, SNe can be detected in distant galaxies. By measuring the cosmic occurrence rate of core-collapse SNe, one can study the overall formation rate of the massive star population through cosmic time. With upcoming or planned large-scale optical and near-infrared (NIR) surveys, SNe could be detected to $z \sim 2$ or higher. It is thus important to derive a realistic estimate for the detectability in order to make an efficient survey strategy for such observational programmes.

Lien & Fields (2009) study the detectability of core-collapse SNe with the *Large Synoptic Survey Telescope* (LSST, Ivezic et al. 2008; LSST Science Collaborations et al. 2009). They show that the wide survey with LSST (with the 5 σ r-band limiting magnitude of 25 mag) can detect Type II SNe, core-collapse SNe with hydrogen features, up to $z \sim 2$. Magnification by gravitational lensing will boost the number of detectable SNe (Oguri & Marshall 2010).

Type II SNe at higher redshifts can be detected by an extremely deep NIR survey (Miralda-Escude & Rees 1997; Mesinger, Johnson & Haiman 2006) with future satellites such as *James Webb Space Telescope* (JWST). Mesinger, Johnson & Haiman (2006) show that up to several thousands Type II SNe can be detected at $z \sim 6$ if the survey depth reaches the flux limit of 3 nJy (30 mag in AB magnitude), which can be achievable with long ($\sim 10^5$ seconds) integration with JWST.

It may be more promising to aim at detecting SNe that are bright in the rest frame optical to ultra-violet (UV) wavelengths. Type IIn SNe, a type of SNe with narrow hydrogen emission lines, are ideal targets to detect at high-redshifts

---

* E-mail: masaomi.tanaka@nao.ac.jp

© — RAS

(Cooke 2008). Type IIn SNe are thought to be powered by the interaction of the SN ejecta with the circumstellar medium (Schlegel 1990), and are bright in the rest frame optical to UV. Cooke et al. (2009) reported the discovery of Type IIn SNe at $z = 2.4$ and 2.0 in the archival data of the legacy survey with Canada-France-Hawaii Telescope.

There is another type of possibly luminous SNe worth mentioning here. Pair-instability SNe (PISNe) are thought to be triggered by very massive stars with mass in the range of 140-260 $M_{\odot}$ at zero metallicity (Heger & Woosley 2002), and are also expected to be very luminous (Scannapieco et al. 2005). PISNe might also occur even in the local Universe, as suggested by the recent discovery of SN 2007bi (Gal-Yam et al. 2009; Young et al. 2010). However, PISNe are not very luminous at rest UV wavelengths (Kasen, Woosley & Heger 2011), and thus they can be detected only at $z < 2$ even with LSST (Pan, Loeb & Kasen 2011). It is possible, in principle, to detect PISNe at $z > 6$ with an extremely deep NIR survey with K =28.7 mag (Scannapieco et al. 2005, see also recent papers by Pan, Kasen & Loeb 2011; Hummel et al. 2011), but the occurence rate of PISNe (or the formation rate of extremely massive stars) at such high redshifts is highly uncertain. Interestingly, recent theoretical studies and detailed simulations of the first generation of stars suggest that the characteristic mass of the first stars is not as large as the progenitor of a PISN (Yoshida, Omukai & Hernquist 2007; Hosokawa et al. 2011). Then observing core-collapse SNe may be a more promising route to study the massive star population in the early Universe.

Recently, superluminous SNe were discovered such as SN 2006gy (Ofek et al. 2007; Smith et al. 2007, 2008; Agnoletto et al. 2009; Kawabata et al. 2009) and SN 2005ap (Quimby et al. 2007), whereas other superluminous SNe include SNe 2003ma (Rest et al. 2011), 2006oz (Leloudas et al. 2012), 2008es (Miller et al. 2009; Gezari et al. 2009), 2008fz (Drake et al. 2010), 2008ma (Chatzopoulos et al. 2011), 2010gx (PTF10cwr, Pastorello et al. 2010; Quimby et al. 2011), SCP 06F6 (Barbary et al. 2009). PTF09atu, PTF09cnd, PTF09cwl, (Quimby et al. 2011), PS1-10ky, PS1-10awh (Chomiuk et al. 2011), and CSS100217 (Drake et al. 2011). See also Richardson et al. (2002) for other earlier candidates. These SNe have an absolute magnitude of about -22 mag in optical. Some of them are classified as Type IIn (e.g., Ofek et al. 2007; Smith et al. 2007), or Type IIL, which is a subclass of Type II SNe with the linear light curve decline (Miller et al. 2009; Gezari et al. 2009), and others are hydrogen poor (Type Ibc, e.g., Pastorello et al. 2010; Quimby et al. 2011).

The nature of these superluminous SNe is poorly known. Some of them are powered by the circumstellar interaction, or by the shock breakout from the dense circumstellar medium (Chevalier & Irwin 2011; Moriya & Tominaga 2011), as suggested by the presence of narrow emission lines in superluminous Type IIn SNe (e.g., Agnoletto et al. 2009). It is also argued that superluminous SNe could be powered by a large amount of ^{56}Ni which is synthesized as a result of energetic core-collapse SNe (Umeda & Nomoto 2008; Young et al. 2010; Moriya et al. 2010). Other scenarios include the interaction between shells ejected by the pulsational pair-instability (Woosley, Blinnikov & Heger 2007), and SNe powered by a magnetar (Maeda et al. 2007; Kasen & Bildsten 2010; Woosley 2010).

Although the origin of the high luminosity is not yet fully understood, the progenitors of the superluminous SNe are thought to be very massive. The long time-scale of the light curve is suggestive of a long diffusion times of optical photons and hence of a large mass of ejecta (for a given kinetic energy). At least one progenitor of Type IIn SN is directly identified to be as luminous as luminous blue variables with the zero-age main sequence mass of $M_{\rm ZAMS} > 50 - 80 M_{\odot}$ (Gal-Yam et al. 2007; Gal-Yam & Leonard 2009).

Superluminous SNe may provide an important information on the star formation in the high-redshift Universe. Because superluminous SNe are likely to be triggered by the very massive end of the stellar population, the relative occurence rate of such SNe with respect to the overall star formation rate can be a sensitive probe of the slope of the stellar initial mass function (IMF). Theoretical studies suggest that the shape of the IMF may be different in the early Universe, or could even be of top-heavy one (e.g., Larson 1998). Detecting superluminous SNe at high redshifts will give a direct evidence for such non-standard IMF.

In this paper, we study the detectability of superluminous SNe at high redshifts with the upcoming wide-field surveys. Quimby et al. (2011) noted that superluminous SNe are bright enough that they can be detectable even at $z \sim 4$ with 8m-class telescopes, such as Subaru and LSST. We derive a realistic estimate for the detectability for a few particular set of surveys. For the optical survey, we focus on the proposed survey with the Subaru/Hyper Suprime-Cam (HSC, Miyazaki et al. 2006). The method of mock observations is described in Section 2. We show that with a realistic survey strategy we can detect superluminous SNe to $z \sim 4 - 5$ (Section 3). More emphasis is made on the detectability by upcoming NIR survey utilizing future satellites, such as Euclid[1], The Wide-Field Infrared Survey Telescope (WFIRST) [2], and Wide-field Imaging Surveyor for High-redshift (WISH) [3] (Section 4). We study how the expected number of detection at $z > 3$ is affected by the slope of the IMF at the massive end. Details of the sample selection are described in Section 5. Finally, we give our concluding remarks in Section 6.

Throughout the paper, we assume the $\Omega_M = 0.3$, $\Omega_\Lambda = 0.7$ and $H_0 = 70$ km s^{-1} Mpc^{-1} cosmology, which is consistent with, e.g., Komatsu et al. (2011). The magnitudes are given in the AB magnitude when nothing is mentioned.

2 SETUP FOR MOCK OBSERVATIONS

We perform simulations of mock observations to study the detectability of superluminous SNe at high redshift. To this end, we need (1) spectral energy distributions (SEDs) of superluminous SNe and their time evolution, (2) cosmic occurrence rate of superluminous SNe, and (3) a few key observational parameters, i.e., the depth, the area, and the cadence of observations. In the following subsections, we describe the setup for our simulations.

---

[1] `http://sci.esa.int/euclid`

[2] `http://wfirst.gsfc.nasa.gov`

[3] `http://www.wishmission.org/en/index.html`

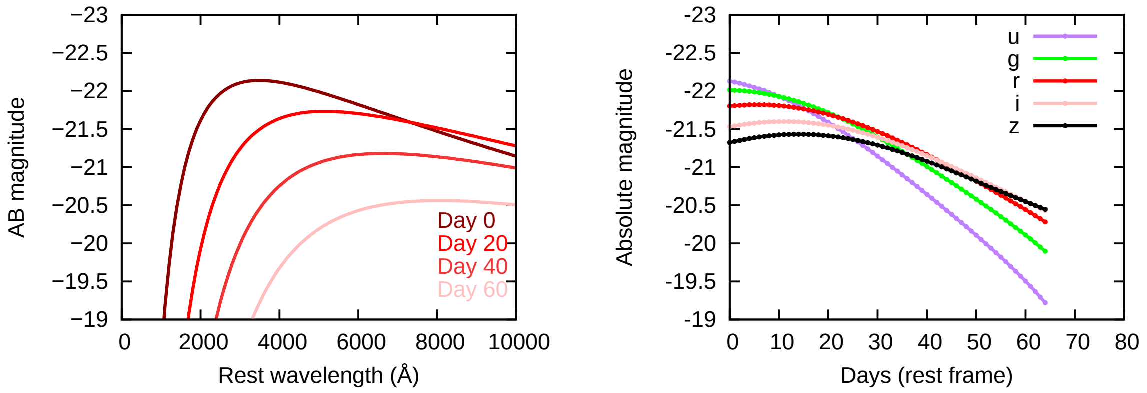

Figure 1. Rest-frame SED (left) and absolute light curves (right) of superluminous SN 2008es, used as the base model of our simulations. The evolution of the luminosity and the effective blackbody temperature are taken from Miller et al. (2009).

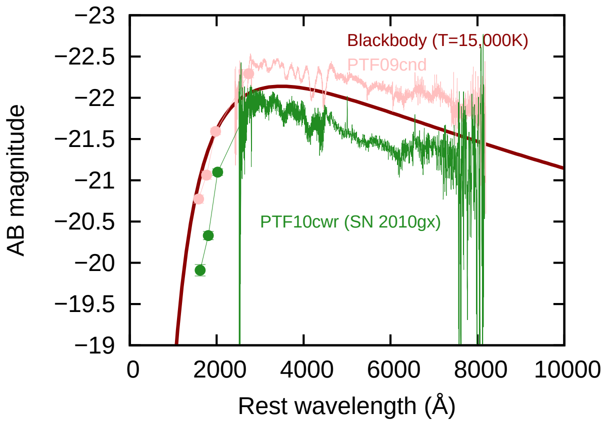

Figure 2. SEDs of hydrogen poor superluminous SNe PTF09cnd (pink) and PTF10cwr (SN 2010gx, green) compared with the blackbody with $T = 15,000$ K. Spectral data are from Quimby et al. (2011) and photometric data are from Quimby et al. (2011); Pastorello et al. (2010).

2.1 SED of Superluminous Supernovae

As our fiducial model, we use the observed SED of SN 2008es (Miller et al. 2009; Gezari et al. 2009). SN 2008es is a well-observed object among superluminous SNe. The SED can be approximately described by blackbody radiation with temperature of $6000 - 15000$ K depending on the phase. We adopt the model by Miller et al. (2009) for the luminosity and the blackbody temperature. Note that the SED is *not* corrected for host galaxy extinction. We assume a cut-off of the flux at the wavelengths shorter than the Lyman limit. The model SED and rest-frame light curves for SN 2008es are shown in Figure 1. Around the maximum brightness, the blackbody temperature is ~ 15000 K, and the peak wavelength is found at about 3000 Å.

It is known that there is a variety of SEDs of superluminous SNe; some SNe show H features while other do not. Figure 2 shows the SEDs of hydrogen poor superluminous SNe PTF09cnd (Quimby et al. 2011) and PTF10cwr (SN 2010gx, Pastorello et al. 2010; Quimby et al. 2011). For comparison, the blackbody spectrum with $T = 15,000$ K is also shown, which is assumed in our fiducial model at the maximum brightness. The overall SEDs are similar at the relevant wavelengths. Quimby et al. (2011) and Chomiuk et al. (2011) also find that the evolution of the effective blackbody temperature is similar among the superluminous SNe. Although the SEDs of SN 2008es may not apply to all the superluminous SNe, it is reasonable to assume that superluminous SNe have a bluer colour than other types of SNe (Quimby et al. 2011).

The characteristic time scale of the luminosity evolution differs among superluminous SNe (see e.g., Figure S1 of Quimby et al. 2011). For example, the bolometric light curve of SN 2008es declines by 0.85 dex in 50 days while that of PTF09cnd declines only 0.25 dex in the same period. Our fiducial model is based on SN 2008es, which yields conservative estimates for the number of detections. We also perform simulations by using the blackbody model for PTF09cnd by Quimby et al. (2011) to see the dependence on the model.

We also note that dense observations of SN 2008es were done only after its maximum brightness. We do not extrapolate the light curve before the maximum (Figure 1), and do not count SNe in the early phase. Consequently, our simulations give conservative estimates. We argue that, if the light curve has a symmetric shape, the number of detections can increase up to by a factor of 2.

SN 2008es has a peak magnitude of -22 mag in g-band, whereas some of superluminous SNe have even a brighter magnitude up to -23 mag (e.g., Quimby et al. 2007, 2011). It is not yet clear if the superluminous SNe are the objects at the luminous end of the luminosity function of normal core-collapse SNe, or they form an independent population. For our simulations, we assume the latter case, and adopt a Gaussian luminosity function with the g-band peak magnitude of -22 mag. Since the dispersion of the peak magnitude is not well constrained, we adopt a small value (0.3 mag) so that the results are not affected by the luminous end of the luminosity function. Note that this luminosity function crudely includes the effect of extinction in the host galaxies, because the host extinction is *not* corrected in most of the literature.

To perform realistic mock observations, we also include Type Ia, Type IIP, and Type Ibc SNe in our simulations. For the SEDs of these types, we use spectral templates by

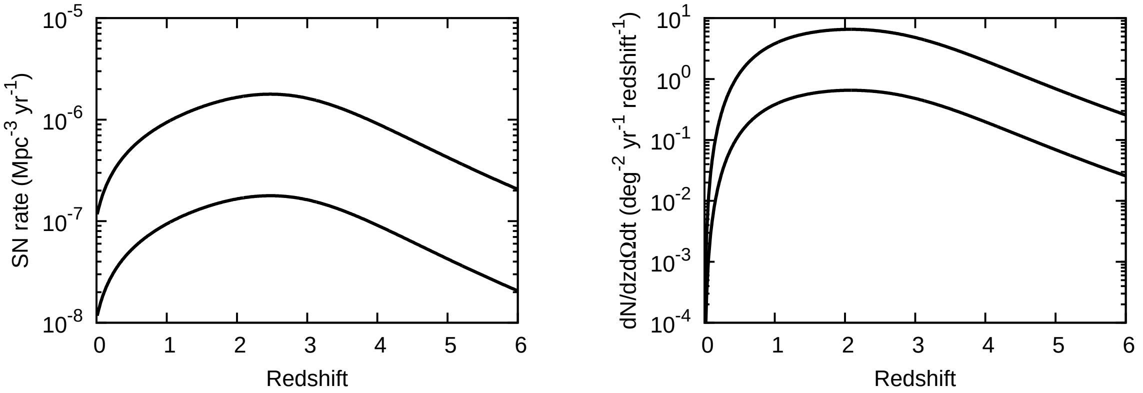

Figure 3. The cosmic occurrence rate of superluminous SNe assumed in the present paper. The left panel shows the rate per volume, while the right panel shows the rate per area per unit redshift. Two solid lines show the cases for $f_{\rm SLSN} = 2 \times 10^{-2}$ (top) and 2×10^{-3} (bottom). See text for the efficiency parameter $f_{\rm SLSN}$.

Nugent, Kim & Perlmutter (2002) [4]. For their luminosity functions, we assume observed average peak R-band Vega magnitudes and dispersion of nearby SNe, i.e., $M_R = -18.6$ mag (σ =0.8 mag), -16.1 mag (σ =1.2 mag) and -16.1 mag (σ =1.4 mag), for Type Ia, IIP and Ibc SNe, respectively (Li et al. 2011).

2.2 Supernova Rate

Superluminous SNe are likely to be the explosions of massive progenitors. It is reasonable to assume that the occurrence rate is proportional to the cosmic star formation rate $\rho_*(z)$ without significant time delay. We assume the minimum zero-age main sequence mass for superluminous SNe to be $M_{\rm min,SLSN} = 50 M_{\odot}$, which is the minimum mass of luminous blue variables (Gal-Yam et al. 2007). Suppose only a small fraction $f_{\rm SLSN}$ of massive stars (with $> 50 M_{\odot}$) explode as superluminous SNe. Then the rate of the superluminous SNe as a function of redshift $R_{\rm SLSN}(z)$ can be calculated as

$$R_{\rm SLSN}(z) = f_{\rm SLSN}\, \rho_*(z) \frac{\int_{M_{\rm min,SLSN}}^{M_{\rm max,SLSN}} \psi(M) {\rm d}M}{\int_{M_{\rm min}}^{M_{\rm max}} M \psi(M) {\rm d}M}, \tag{1}$$

where $\psi(M)$ is the stellar IMF

$$\psi(M) \propto M^{-(\Gamma+1)}. \tag{2}$$

We adopt a modified Salpeter A IMF of Baldry & Glazebrook (2003) with the slope $\Gamma = 0.5$ for $0.1 M_{\odot} < M < 0.5 M_{\odot}$ and $\Gamma = 1.35$ for $0.5 M_{\odot} < M < 100 M_{\odot}$. The other parameters in Eq. (1) are, the minimum mass of stars $M_{\rm min} = 0.1 M_{\odot}$, the maximum mass of stars $M_{\rm max} = 100 M_{\odot}$, and the maximum mass of superluminous SNe $M_{\rm max,SLSN} = 100 M_{\odot}$. For the star formation rate, we use the parametrized prescription by Hopkins & Beacom (2006) with a modified Salpeter A IMF.

The fraction of superluminous SNe, $f_{\rm SLSN}$, is not well determined. It is indeed one of the important goals of upcoming surveys to anchor the rate of such events to understand the population of progenitors. In the present paper, we calibrate this fraction with the available observations so far. Quimby et al. (2011) estimated the rate of hydrogen poor superluminous SNe to be about 10^{-8} Mpc^{-3} yr^{-1} at $z \simeq 0.3$, which is only 10^{-4} of total core-collapse SNe. This fraction corresponds to $f_{\rm SLSN} = 2 \times 10^{-3}$ of massive stars with $> 50 M_{\odot}$. Including hydrogen rich superluminous SNe, such as superluminous Type IIn SNe, the rate can be higher. Thus, in our simulations, we adopt $f_{\rm SLSN} = 2 \times 10^{-3}$ - 2×10^{-2}, i.e., 10^{-4} - 10^{-3} of total core-collapse SNe are superluminous SNe.

The left panel of Figure 3 shows the rate of the superluminous SNe. The rate lies roughly between 10^{-7} and 10^{-6} Mpc^{-3} yr^{-1} in the redshift range we are most interested in. The SN rate per volume per year can be readily converted to the number per redshift per field (solid angle Ω) and per a certain duration of observations as

$$\frac{{\rm d}N}{{\rm d}\Omega\, {\rm d}t\, {\rm d}z} = R_{\rm SLSN}(z) \frac{1}{1+z} \frac{{\rm d}V_{\rm com}}{{\rm d}\Omega {\rm d}z}, \tag{3}$$

where $V_{\rm com}$ is the comoving volume. The right panel of Figure 3 shows the number of SNe per 1 square degree, per 1 year, and per redshift. The number of superluminous SNe at $z \sim 2$ is about unity within 1 deg^2 per year, and does not decrease significantly to $z \sim 4$.

2.3 Survey Strategy

We primarily consider three types of surveys with different survey area, depth, cadence, and wavelength (Table 1). In practice, deep imaging observations must be performed before each survey to make a reference image. The transient survey described below will be performed after such reference observations.

First, we adopt the proposed parameters for the deep layer of the Subaru/HSC survey (hereafter called HSC-Deep). The survey is planned to cover 30 deg^2. The same field will be visited twice per month with a 6-day cadence around the new-moon phase. Such observations will be repeated for continuous 3 months.

We define the survey cadence with 3 parameters; n_1 and Δt are the number of visits and its cadence within one month, and n_2 is the number of monthly visits. Thus, for HSC-Deep, $n_1 = 2$, $\Delta t = 6$ days, and $n_2 = 3$.

---

[4] `http://supernova.lbl.gov/~nugent/nugent_templates.html`

Table 1. Survey Parameters

Survey	Area (deg^2)	Δt (day)	n_1	n_2	5 σ limiting magnitude per visit				
					m_g	m_r	m_i	m_z	m_y
Subaru/HSC Deep	30	6	2	3	26.1	25.8	25.6	24.5	23.2
Subaru/HSC Ultra Deep	3.5	6	3	4	26.9	26.6	26.6	25.6	24.3
					m_{F115W}	m_{F200W}	m_{F277W}	m_{F356W}	m_{F444W}
NIR Deep	100	–	1	6	26.0	26.0	26.0	26.0	26.0

The HSC survey is proposed to be performed with 5 broad band filters (g, r, i, z, and y). The planned survey depth is summarized in Table 1. For HSC-Deep, the exposure time required to reach the designated depths is 12 min for g and r bands, and 18 min for i, z, and y bands.

The second survey we consider is the Ultra Deep layer of Subaru/HSC survey (hereafter HSC-UltraDeep). It will observe two Subaru/HSC fields (3.5 deg^2 in total) with deeper magnitude limits and more frequent cadence (see Table 1). The required exposure times for these limits are 30 min, 30 min, 60 min, 90 min, and 90 min for g, r, i, z, and y band, respectively. The same field will be observed 3 times per month with a 6-day cadence, and this sequence will be repeated for 4 months, i.e., $n_1 = 3$, $\Delta t = 6$ days, and $n_2 = 4$.

Finally, we explore SN detection by NIR surveys. We propose a hypothetical survey with a wide area of 100 deg^2, which will be made possible by future satellite missions such as Euclid, WFIRST and WISH. For the transmission curve of NIR filters, the broad band filters of JWST are used [5]. We assume a constant depth of 26.0 mag for 5 bands in 1-5 μm. For the NIR survey, we assume only one visit per month ($n_1 = 1$) for continuous 6 months ($n_2 = 6$).

2.4 Methods of Simulations

In this subsection we describe the details of our mock observations. We first generate superluminous SNe according to the SN rate in the right panel of Figure 3 and the adopted survey area assumed for each survey strategy. The observed light curve of each superluminous SN at a certain redshift is calculated from the SED in Figure 1 with appropriate K-correction (Hogg et al. 2002). Here the luminosity of each SN is assigned according to the luminosity function (with a Gaussian probability distribution). The date of explosion is determined by a random number. In this way, we generate expected light curves of superluminous SNe at a range of redshifts.

Then we perform mock observations. The magnitude of superluminous SNe are compared with the limiting magnitude of the survey specified by $\Delta t, n_1$ and n_2 (see Table 1). We do not consider contamination of the host galaxy, i.e., the detection limit in Table 1 is kept constant for all the objects. Strictly speaking, this is not the case when an object is discovered near a bright galaxy. However, for high-redshift superluminous SNe, the host galaxies are expected to be faint (Section 5), and thus it is a sound approximation to neglect the contamination.

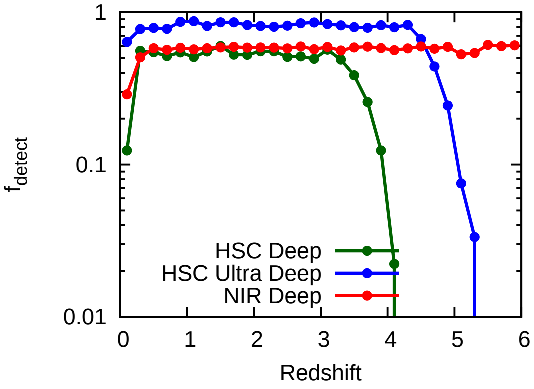

Figure 4. Detection efficiency of superluminous SNe as a function of redshift for HSC-Deep (green) and HSC-UltraDeep (blue), and for a hypothetical NIR deep survey (red).

We impose stringent detection criteria. Only SNe that fulfill *both* of the following two criteria are counted as "detected"; (1) brighter than 5 σ detection limit in more than 2 bands at least at one epoch, and (2) brighter than the 5 σ detection limit at more than 3 epochs at least in one band. Typically, we generate light curves for 1000 superluminous SNe per one run. The simulations are performed 1000 times, and the number of the detection is averaged over the realizations.

3 DETECTABILITY WITH OPTICAL SURVEY

We first calculate the detection efficiency for the three surveys we propose. The detection efficiency is defined to be the ratio of the detected number of SNe to the total number of SNe exploded in the survey period. The green and blue lines in Figure 4 show the detection efficiency (f_{detect}) of superluminous SNe for HSC-Deep and HSC-UltraDeep, respectively. We see rapid drop in f_{detect} at $z \sim 3-4$ and $z \sim 4-5$ for Deep and for Ultra Deep, respectively. These limiting redshifts corresponds to the redshifts where superluminous SNe with the mean absolute magnitude -22 mag becomes undetectable in z-band (see Appendix A for the SEDs in observer's frame). HSC-Deep is almost complete up to $z \sim 3$ while HSC-UltraDeep is complete up to $z \sim 4$. The efficiency at lower redshift is not unity because of our somewhat stringent detection criteria. If we impose a looser

---

[5] `http://www.stsci.edu/jwst/instruments/nircam/instrumentdesign/filters/index_html`

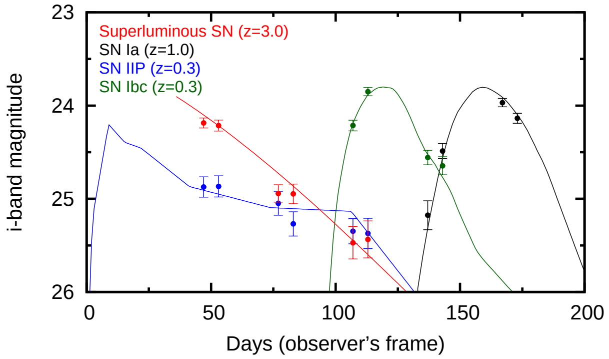

Figure 5. An example of the simulated i-band light curve of a superluminous SN (red) for HSC-Deep. The light curve is compared with that of Type Ia (black), Type IIP (blue), and Type Ibc (green) SNe at lower redshifts. Photometric errors shown here are computed according to the limiting magnitudes in Table 1. The light curves of Type Ia SNe and Type Ibc SNe are shifted toward the right for clarity.

criteria, for example, $> 5\sigma$ detection at only 2 epochs, the efficiency becomes nearly unity at low redshifts. The efficiency and its redshift dependence are not largely affected even when PTF09cnd, which has a slower light curve than our fiducial model, is used as our input model.

It is worth mentioning that SNe exploded before the survey period can also be detected. This effect is not included in the detection efficiency, but such SNe are included in the detection number shown below.

Figure 5 shows a few examples of simulated light curves. Photometric errors are computed according to the limiting magnitudes in Table 1. The i-band light curve of a superluminous SNe is shown by the red points. It is compared with those of other types of SNe. Superluminous SNe at $z \sim 3$ have comparable magnitude with other types of SNe at $z \lesssim 1$. Since the observed i-band wavelength corresponds to the rest-UV wavelengths, the decline rate of superluminous SNe is not extremely long. The observed time-scale is slightly longer than that of Type Ia and Ibc SNe, but shorter than that of Type IIP SNe at plateau phase.

When PTF09cnd is used as input, the observed brightness of a model superluminous SN at $z = 3$ decreases as slowly as that of Type IIP SNe at $z = 0.3$. In this case, about 50 % of the superluminous SNe detected with the HSC-Deep do not show the variability larger than 1 mag in any band. [6] It is thus important to have deep reference images before the survey, otherwise such SNe would be missed.

The expected number of detection of superluminous SNe with each layer of the survey is shown in Figure 6. Two solid lines show the cases for $f_{\rm SLSN} = 2 \times 10^{-2}$ (top) and 2×10^{-3} (bottom). Our reasonable guess is that the true number will lie in between them. The total number of detection is 15-150 for the Deep layer, and 3-30 for the Ultra Deep layer. If PTF09cnd is used as input, these numbers increase by 20 % because of the slow luminosity evolution.

For both the layers, the median redshift is found to be $z \sim 2$, where the star formation rate and hence the intrinsic SN rate has a peak. The wider survey area of HSC-Deep gives a larger number of detection at $z = 1-3$. In the future, a dedicated deep survey by LSST will discover more superluminous SNe. If a similar depth is achieved, for example, in the deep drilling field (LSST Science Collaborations et al. 2009), the expected number of detection is simply proportional to the survey area.

We expect that the rate of superluminous SNe at $z \sim 1-3$ is accurately determined with HSC-Deep. HSC-UltraDeep can possibly detect superluminous SNe even at $z \sim 5$ if $f_{\rm SLSN} = 2\times10^{-2}$. This is in contrast to PISNe, which we can detect only at $z < 2$ with LSST (Pan, Loeb & Kasen 2011). The highest redshift of superluminous SNe depends on the intrinsic rate of superluminous SNe, which can be observationally constrained by HSC-Deep. We emphasize that surveys with the 2 layers are important to understand first the properties of the superluminous SNe (Deep layer) and then to detect highest-redshift SNe (Ultra Deep layer).

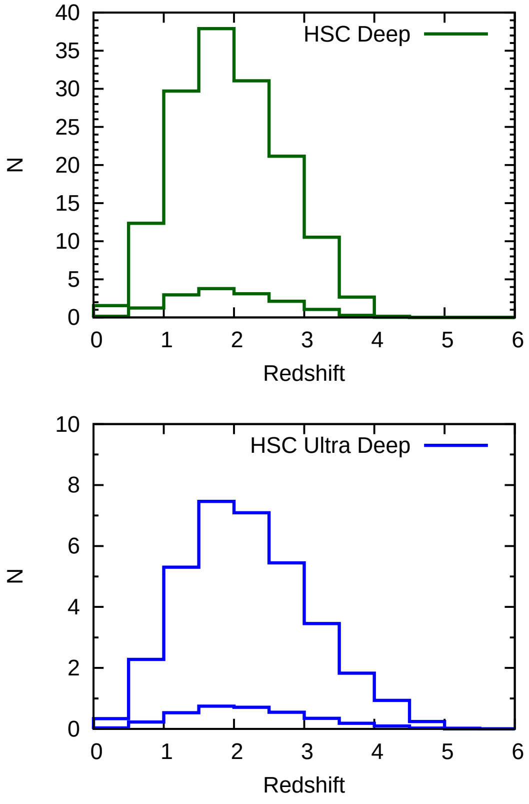

Figure 6. Expected number of detection as a function of redshift for HSC-Deep (upper panel) and HSC-UltraDeep (lower panel). The two solid lines show the cases for $f_{\rm SLSN} = 2 \times 10^{-2}$ (top) and 2×10^{-3} (bottom). The total number of detection is 15-150 for HSC-Deep and 3-30 for HSC-UltraDeep.

---

[6] The fraction of SNe with a small variability (< 1 mag) is only $\sim$ 15 % when the model of SN 2008es is used. This fraction becomes smaller if the baseline the survey period is longer. For example, if the HSC-Deep is performed over 6 months keeping the total number of visit, i.e., $n_1 = 1$ and $n_2 = 6$, the fraction of the small variability case is only 20 % for the PTF09cnd model, and almost 0 % for the SN 2008es model.

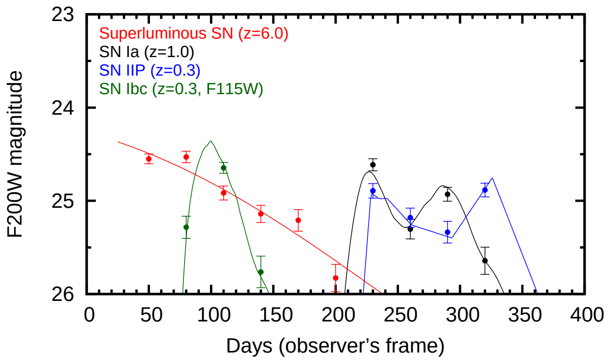

Figure 7. NIR light curves of superluminous SNe (red) compared with Type Ia (black), IIP (blue), and Ibc (green) SNe. For superluminous SNe, Type Ia and IIP SNe, magnitudes in the F200W filter is shown. Since the SED of Type Ibc SNe at 2μm is uncertain (see Figure A1), magnitudes in the F115W filter is shown for Type Ibc SNe. The light curves of Type Ia SNe and Type IIP SNe are shifted toward the right for clarity.

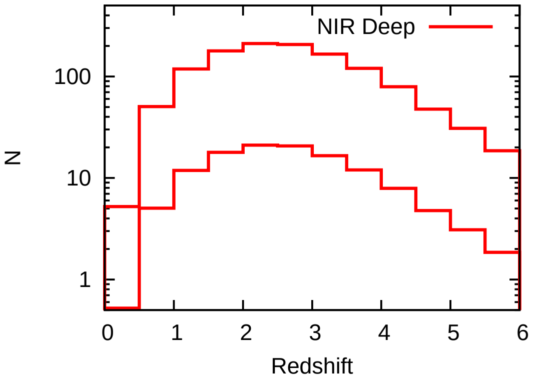

Figure 8. Expected number of detection as a function of redshift for the 100 deg^2 NIR survey. The two solid lines show the cases for $f_{\mathrm{SLSN}} = 2 \times 10^{-2}$ (top) and 2×10^{-3} (bottom). The total number of detection is 120-1200.

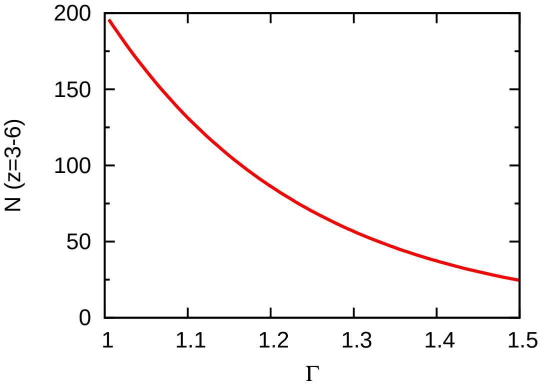

Figure 9. Expected cumulative number of superluminous SNe at $z > 3$ as a function of the sloop index Γ of the IMF at $M > 50 M_{\odot}$. For this plot, our 'conservative' SN rate ($f_{\mathrm{SLSN}} = 2 \times 10^{-3}$) is assumed.

4 NIR SURVEY

4.1 Expected Number of Detection

It is likely that a NIR survey is more efficient than the optical surveys to detect high redshift superluminous SNe. The red line in Figure 4 shows the detection efficiency for our proposed NIR survey. The efficiency is approximately constant at $z = 0 - 6$. The maximum efficiency is 0.5 simply because we require detection at 3 epochs. Most superluminous SNe up to $z \sim 6$ are above the detection limit. However, because of our criteria, superluminous SNe occured in the latter 3 months in the survey period are not included in Figure 4. Using NIR bands is essential to perform a complete survey at redshift $z > 3$.

Figure 7 shows the simulated light curves of superluminous SNe (red) compared with other types of SNe. Thanks to the high rest-UV luminosity (Figure 1), superluminous SNe even at $z = 6$ can be as bright as 24-25 mag at 2 μm. Because of the time dilation, the light curve of superluminous SNe at high redshifts has a long time-scale in NIR.

The expected number of detection is shown in Figure 8. It is highly interesting that, with a 100 deg^2 survey, hundreds of $z > 2$ SNe can possibly be discovered. The total number of SNe is 120 and 1200 for the cases of $f_{\mathrm{SLSN}} = 2 \times 10^{-3}$ and 2×10^{-2}, respectively. We discuss the usefulness of such a large sample at high redshifts in the next subsection.

4.2 Sensitivity to the IMF

As we mentioned earlier, the superluminous SNe of our target are thought to be triggered by very massive stars. The occurrence rate is very sensitive to the number fraction of such massive stars. This in turn can be used, if the occurence rate is accurately determined, to probe the slope of the IMF at the massive end (Cooke et al. 2009). We calculate the sensitivity of the expected number of the detection to the slope of the stellar IMF. For simplicity, we fix the minimum mass of superluminous SNe ($M_{\mathrm{min,SLSN}}$) and the fraction of superluminous SNe (f_{SLSN}) for the following comparison. Note that these parameters can be observationally constrained by the optical survey as we discussed in Section 3. To study the influence of the relative fraction of massive stars, we change the slope of the IMF at the large mass $> 50 M_{\odot}$, whereas keeping the slope at $< 50 M_{\odot}$ to be 1.35. It is important to note that changing the IMF at the high-mass end has little impact to the calibration of the star formation rate since most UV continuum emission comes from massive stars with $< 50 M_{\odot}$. Thus the occurence rate of superluminous SNe is a robust probe of the stellar IMF.

Figure 9 shows the cumulative number of detection at $z = 3 - 6$ as a function of Γ, the slope of the IMF. Here the fraction of superluminous SNe is conservatively assumed to be $f_{\mathrm{SLSN}} = 2 \times 10^{-3}$. Even in this case, with $\Gamma < 1.1$, the expected number can be about three times as much as that with $\Gamma = 1.35$. Thus, if the star formation rate is independently measured, and if the SN rate can be determined with an accuracy within a factor of 3, the very flat slope of the massive end of the IMF can be inferred, or rejected.

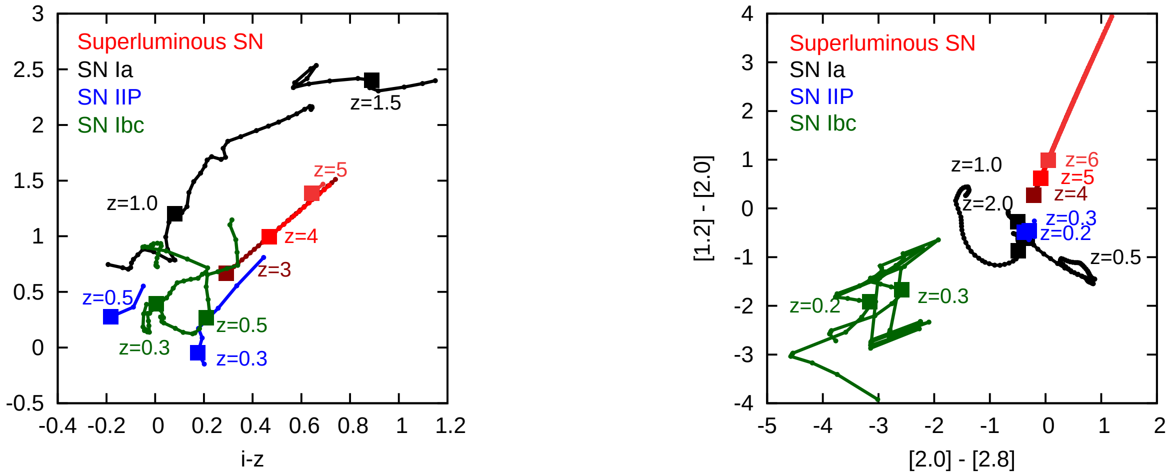

Figure 10. Optical (left) and NIR (right) colour-colour diagram for various types of SNe. Our template superluminous SN 2008es at high redshifts (red) are compared with Type Ia SNe (black), Type IIP SNe (blue), and Type Ibc SNe (green) at low redshifts. The redshift of Type Ia, IIP, and Ibc SNe are selected so that the observed magnitudes are similar to those of high-redshift superluminous SNe. Colours at different epochs are connected with lines, and the square shows the colour at maximum brightness. In optical, colours of superluminous SNe at high redshifts are red both in $r-i$ and $i-z$, compared with Type IIP SNe and Type Ibc SNe. Only Type Ia SNe at redshift $z = 1.5$ can have colours redder than superluminous SNe both in $r-i$ and $i-z$. In NIR, superluminous SNe at high redshifts are redder than any other types of SNe with similar observed brightness. For the detailed SED, see Appendix A.

5 NOTES ON THE SAMPLE SELECTION

So far we have discussed the number of detectable SNe of a particular type, but have not fully evaluated the efficiency of target selection for actual surveys. Because superluminous SNe are intrinsically rare events, upcoming optical surveys using 8m-class telescope, such as Subaru and LSST, and NIR surveys with Euclid, WFIRST, and WISH, will discover more Type Ia and ordinary core-collapse SNe. These normal SNe will be more abundant than superluminous SNe by a factor of about 100. Thus, to identify superluminous SNe at high redshifts, we must select the candidates properly and efficiently.

Cooke (2008) propose a method to select Type IIn SNe from colour-selected Lyman break galaxies. The advantage of the method is that the photometric redshift of the host galaxy is already known. When Lyman break galaxies at $z > 2$ are selected, most of SN candidates found in this sample are likely to be Type IIn SNe or superluminous SNe.

Here we consider the characteristics of superluminous SNe in a more general case. An important issue would be that the host galaxy of a distant SNe is likely to be too faint to be detected. We summarize the properties of (1) light curve and its time scale, (2) colours, and (3) host galaxies of superluminous SNe at high redshifts.

The observed time-scale is determined by the intrinsic time-scale and the time dilation due to cosmological redshift. Superluminous SNe observed so far indeed tend to show an intrinsically long time-scale. For an extreme case, the brightness of SN 2006gy stayed within 1 magnitude below the maximum for about 100 days. Other objects such as 2008es (Miller et al. 2009; Gezari et al. 2009), SCP 06F6 (Barbary et al. 2009). PTF09atu, PTF09cnd, PTF09cwl (Quimby et al. 2011) also have a long time-scale. Their decline tends to be faster in bluer bands (Figure 1).

In optical surveys, we observe high-redshift superluminous SNe at the rest-UV wavelengths. The observed time-scale of superluminous SNe is slightly longer than that of Type Ia and Ibc SNe, and shorter than Type IIP SNe (Figure 5), when we use SN 2008es as a template. When we use PTF09cnd as a template instead, the light curve is as slow as Type IIP SNe. With such a slowly evolving light curve, it may be difficult to distinguish superluminous SNe from Type IIP SNe.

In NIR surveys, the long time-scale of superluminous SNe is pronounced (Figure 7). Since NIR wavelengths traces the rest-frame optical at $z \gtrsim 2$, superluminous SNe at $z \gtrsim 2$ can stay detectable for more than 100 days thanks to both the intrinsic brightness and the dilation effect (Figure 7). As a result, the time-scale is longer than any other types of SNe.

The second diagnostic is the observed colour. Figure 10 shows optical $r - i$ vs. $i - z$ (left) and NIR F115W-F200W ([1.2]-[2.0]) vs. F200W-F277W ([2.0]-[2.8], right) colour-colour diagrams. Colours of our template superluminous SN 2008es at high redshifts are shown in red. For comparison, we also show the expected colours of Type Ia SNe at $z = 1.0$ and 1.5 (black), Type IIP SNe at (blue), and Type Ibc SNe (green) at $z = 0.3$ and 0.5. These SNe are expected to have similar observed magnitudes to those of superluminous SNe at $z > 3$. The colours of these types of SNe are calculated by using the spectral templates by Nugent, Kim & Perlmutter (2002). See Appendix A for the SEDs. The reddening in the host galaxy is *not* taken into account here. It is worth mentioning that there is a scatter in optical colour of observed SNe at low redshifts. Including the contribution from the host galaxy, the scatter is typically about 1.0 mag for Type IIP and 0.5 mag for Type Ibc SNe (e.g., Olivares E. et al. 2010; Drout et al. 2011). For Type Ia SNe, a wide color spread is known, but most objects have similar colours within 0.2-0.4 mag (e.g., Wang et al. 2009).

Superluminous SNe at high redshifts tend to have redder colour than Type IIP and Ibc SNe both in $r-i$ and $i-z$.

For superluminous SNe at high redshifts, the observed r, i, z wavelengths correspond to the near-UV wavelengths in the rest frame, which are at the blueside of the spectral peak. On the other hand, most of Type IIP and Ibc SNe with optical surveys will be discovered at $z \lesssim 1$. Their observed $r-i$ and $i-z$ colours still trace the optical wavelengths in the rest frame. Thus, colours of superluminous SNe at high redshifts tend to be redder than those of Type IIP and Ibc SNe (see also Appendix A). In optical wavelengths, only Type Ia SNe at $z \gtrsim 1$ have a similarly red or redder colour than superluminous SNe. [7]

The red colour of superluminous SNe is more prominent in NIR wavelengths. See the right panel of Figure 10. NIR wavelengths traces the blue optical or near UV wavelength of superluminous SNe at high redshifts (see Appendix A). For other types of SNe, observed NIR wavelengths correspond to the red optical (Type Ia) or NIR (Type IIP and Ibc) in their rest frames. Therefore, NIR colours of superluminous SNe at high redshifts tend to be redder than those of other types of SNe. The red colour of superluminous SNe results simply from the fact that they are at high redshifts. Thus, their red color does not depend largely on the choice of the template SEDs.

The last characteristic is the faintness of the host galaxies of superluminous SNe. An obvious reason for this is the distance to the host galaxies. Interestingly, Neill et al. (2011) argue that the host galaxies of superluminous SNe have a faint intrinsic luminosity; most of them have an absolute r-band magnitudes of $\gtrsim -20$ mag [8]. They also have quite blue UV-optical colours $NUV - r = 0$. If there is no redshift evolution in the host galaxy population, the optical magnitudes of the host galaxies at $z \gtrsim 3$ are likely to be close to the detection limit. This is in contrast to Type Ia SNe at $z = 1 - 1.5$, whose host galaxies were identified in optical wavelengths with m_i = 23-26 mag (Graur et al. 2011). Overall, faintness or non-detection of the host galaxies of the high redshift superluminous SNe may indeed be of help with sample selection in addition to the characteristic features in the light curve and colour.

6 CONCLUSIONS

We study the detectability of superluminous SNe with upcoming optical and NIR surveys. By assuming that the progenitors of superluminous SNe are more massive than 50 $M_\odot$ and a fraction $f_{\rm SLSN} = 2 \times 10^{-3}$ - 2×10^{-2} of these massive stars explode as superluminous SNe (or the rate of superluminous SNe are 10^{-4} - 10^{-3} of total core-collapse SNe), the cosmic occurrence rate of superluminous SNe is about 0.5-5 deg^{-2} yr^{-1} redshift^{-1} at $z \sim 1-3$ and about 0.1-1 deg^{-2} yr^{-1} redshift^{-1} at $z \sim 4-5$.

We predict that 15-150 superluminous SNe up to $z \sim 4$ will be detected with the Deep layer of the upcoming Subaru/HSC survey if all the objects meeting our detection criteria are indeed selected. About the half of them are at $z > 2$. By the Deep layer, the cosmic occurrence rate of superluminous SNe at $z \sim 2-3$ can be anchored. The Ultra Deep layer will discover a smaller number of SNe (3-30), but SNe at $z \sim 5$ could be detectable. A similarly deep, dedicated survey by LSST will discover more superluminous SNe, whose number is simply proportional to the survey area.

We show that future NIR surveys will detect more than a few hundreds of superluminous SNe in half a year if 100 deg^2 field is surveyed with the depth of 26 mag. Even with the conservative estimate of the rate (2×10^{-3} of massive stars with $> 50 M_\odot$, or 10^{-4} of total core-collapse SNe), such NIR survey will detect about 50 superluminous SNe at $z > 3$.

Superluminous SNe at high redshifts can be selected in the sample of high-redshift galaxies as demonstrated by Cooke (2008). Also in the general survey, covering all redshift ranges, superluminous SNe can be distinguished by other types of SNe by (1) the observed long time-scale especially, (2) the optical colour redder than Type IIP and Ibc SNe, or the NIR colour redder than any other types of SNe, and (3) faint host galaxies.

Detection of high-redshift SNe opens an exciting opportunity to study the massive star population at high redshifts. The progenitor of superluminous SNe is likely to be very massive. Therefore, the detected number is very sensitive to the IMF. If the slope of the IMF is $\Gamma < 1.1$ at the high mass end ($M > 50 M_\odot$), the detected number will be increased by a factor of >3. If the star formation rate at $z > 3$ is measured with a small uncertainty by other methods, the detected number of superluminous SNe with the NIR survey can be an indicator of top-heavy IMF at the high-redshift Universe.

The authors thank Robert Quimby for giving us the spectra of PTF09cnd and PTF10cwr, and for fruitful discussion. We thank the anonymous referee for valuable comments that improved our manuscript. We also thank Toru Yamada, Tomoki Morokuma, Nozomu Tominaga and Richard Ellis for useful comments, and Subaru/HSC transient working group for valuable discussion. M.T., T.J.M and N.Y. are supported by the Japan Society for the Promotion of Science (22840009:MT, 23.5929: TJM, 20674003:NY). This research has been supported in part by World Premier International Research Center Initiative, MEXT, Japan.

REFERENCES

Agnoletto I. et al., 2009, ApJ, 691, 1348
Baldry I. K., Glazebrook K., 2003, ApJ, 593, 258
Barbary K. et al., 2009, ApJ, 690, 1358
Chatzopoulos E. et al., 2011, ApJ, 729, 143
Chevalier R. A., Irwin C. M., 2011, ApJ, 729, L6+
Chomiuk L. et al., 2011, ApJ, 743, 114
Cooke J., 2008, ApJ, 677, 137

---

[7] It is worth mentioning here the expected optical colours of quasars as possible contaminations. Most quasars at $z < 4$ have $r - i = -0.5$ - 0.5 and $i - z = -0.5$ - 0.5 (Schneider et al. 2007), which are bluer than superluminous SNe at high redshifts. Quasars at $z = 4 - 5$ have a red $r - i$ colour (up to ~ 2), which is comparable to the colour of superluminous SNe and Type Ia SNe.

[8] Note however that there could be an observational bias that superluminous SNe are easily detected if their host galaxies are faint.

Cooke J., Sullivan M., Barton E. J., Bullock J. S., Carlberg R. G., Gal-Yam A., Tollerud E., 2009, Nature, 460, 237
Drake A. J. et al., 2011, ApJ, 735, 106
—, 2010, ApJ, 718, L127
Drout M. R. et al., 2011, ApJ, 741, 97
Gal-Yam A., Leonard D. C., 2009, Nature, 458, 865
Gal-Yam A. et al., 2007, ApJ, 656, 372
—, 2009, Nature, 462, 624
Gezari S. et al., 2009, ApJ, 690, 1313
Graur O. et al., 2011, MNRAS, 417, 916
Heger A., Woosley S. E., 2002, ApJ, 567, 532
Hogg D. W., Baldry I. K., Blanton M. R., Eisenstein D. J., 2002, arXiv:astro-ph/0210394
Hopkins A. M., Beacom J. F., 2006, ApJ, 651, 142
Hosokawa T., Omukai K., Yoshida N., Yorke H. W., 2011, Science, 334, 1250
Hummel J., Pawlik A., Milosavljevic M., Bromm V., 2011, arXiv:1112.5207
Ivezic Z. et al., 2008, arXiv:0805.2366
Kasen D., Bildsten L., 2010, ApJ, 717, 245
Kasen D., Woosley S. E., Heger A., 2011, ApJ, 734, 102
Kawabata K. S., Tanaka M., Maeda K., Hattori T., Nomoto K., Tominaga N., Yamanaka M., 2009, ApJ, 697, 747
Komatsu E. et al., 2011, ApJS, 192, 18
Larson R. B., 1998, MNRAS, 301, 569
Leloudas G. et al., 2012, submitted to A&A, arXiv:1201.5393
Li W. et al., 2011, MNRAS, 412, 1441
Lien A., Fields B. D., 2009, J. Cosmology Astropart. Phys., 1, 47
LSST Science Collaborations et al., 2009, arXiv:0912.0201
Maeda K. et al., 2007, ApJ, 666, 1069
Mesinger A., Johnson B. D., Haiman Z., 2006, ApJ, 637, 80
Miller A. A. et al., 2009, ApJ, 690, 1303
Miralda-Escude J., Rees M. J., 1997, ApJ, 478, L57+
Miyazaki S. et al., 2006, in Society of Photo-Optical Instrumentation Engineers (SPIE) Conference Series, Vol. 6269, Society of Photo-Optical Instrumentation Engineers (SPIE) Conference Series
Moriya T., Tominaga N., Tanaka M., Maeda K., Nomoto K., 2010, ApJ, 717, L83
Moriya T. J., Tominaga N., 2011, ApJ, in press, arXiv:1110.3807
Neill J. D. et al., 2011, ApJ, 727, 15
Nugent P., Kim A., Perlmutter S., 2002, PASP, 114, 803
Ofek E. O. et al., 2007, ApJ, 659, L13
Oguri M., Marshall P. J., 2010, MNRAS, 405, 2579
Olivares E. F. et al., 2010, ApJ, 715, 833
Pan T., Kasen D., Loeb A., 2011, arXiv:1112.2710
Pan T., Loeb A., Kasen D., 2011, arXiv:1111.3648
Pastorello A. et al., 2010, ApJ, 724, L16
Quimby R. M., Aldering G., Wheeler J. C., Höflich P., Akerlof C. W., Rykoff E. S., 2007, ApJ, 668, L99
Quimby R. M. et al., 2011, Nature, 474, 487
Rest A. et al., 2011, ApJ, 729, 88
Richardson D., Branch D., Casebeer D., Millard J., Thomas R. C., Baron E., 2002, AJ, 123, 745
Scannapieco E., Madau P., Woosley S., Heger A., Ferrara A., 2005, ApJ, 633, 1031
Schlegel E. M., 1990, MNRAS, 244, 269
Schneider D. P. et al., 2007, AJ, 134, 102
Smith N. et al., 2008, ApJ, 686, 485
—, 2007, ApJ, 666, 1116
Umeda H., Nomoto K., 2008, ApJ, 673, 1014
Wang X. et al., 2009, ApJ, 699, L139
Woosley S. E., 2010, ApJ, 719, L204
Woosley S. E., Blinnikov S., Heger A., 2007, Nature, 450, 390
Yoshida N., Omukai K., Hernquist L., 2007, ApJ, 667, L117
Young D. R. et al., 2010, A&A, 512, A70+

APPENDIX A: OBSERVED SEDS OF SUPERNOVAE

Figure A1 shows observed f_ν flux at maximum brightness in the unit of AB magnitude for various types of SNe at various redshifts. The red lines show SEDs of superluminous SN (SN 2008es). SEDs of Type Ia SN (black), Type IIP SN (blue), and Type Ibc SN (green) at most probable redshifts are shown in comparison. Circles shows the values of photometry (u, g, r, i, z, and y for optical, and F115W, F200W, F277W, F356W, and F444W for NIR). In this figure, we assume peak V-band Vega magnitudes that are brighter than the average (Li et al. 2011); $M_V = -19.2$ mag, -16.4 mag and -16.4 mag for Type Ia, IIP and Ibc SNe, respectively.

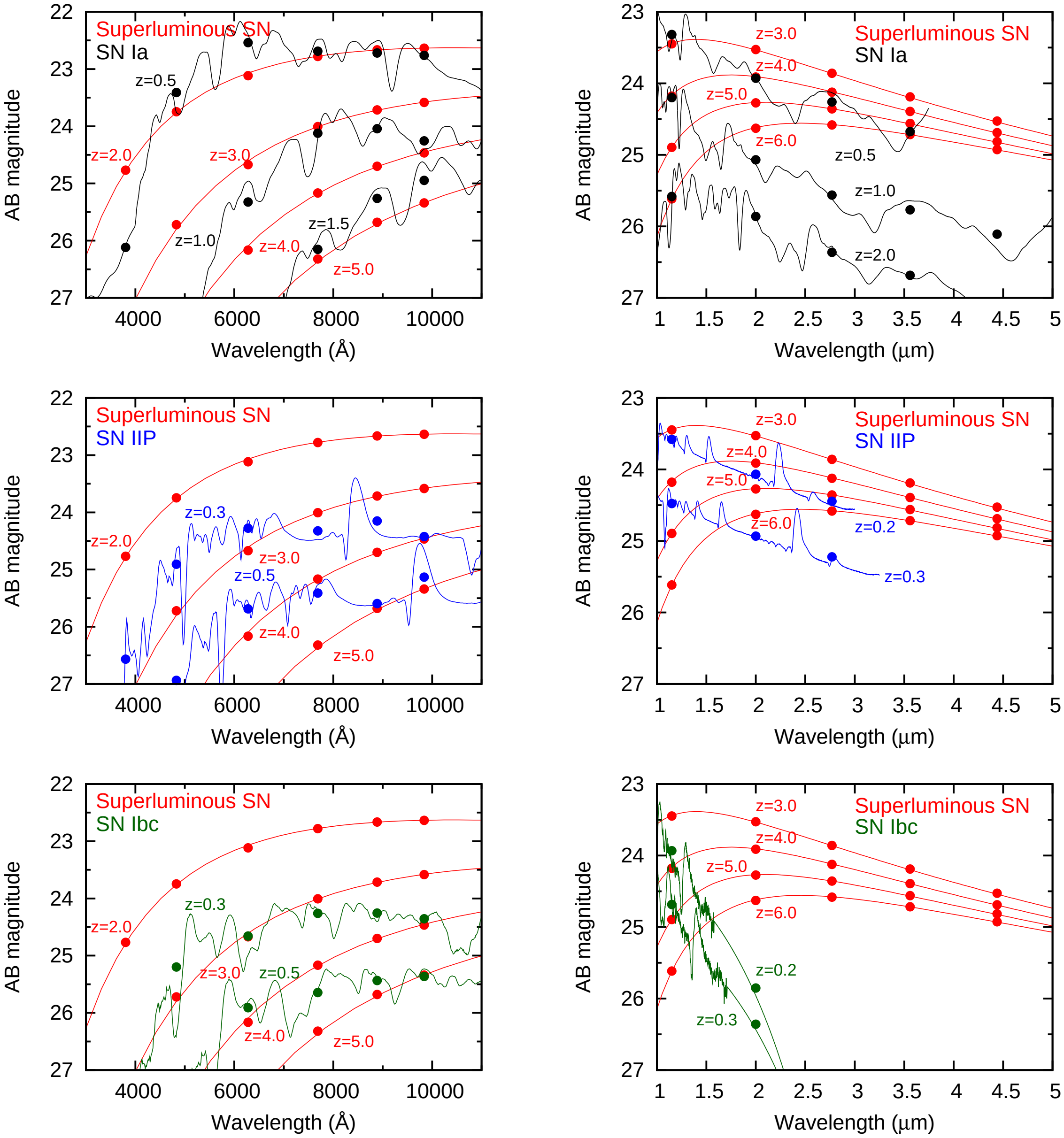

Figure A1. SEDs of various types of SNe at maximum brightness at different redshifts. SEDs of superluminous SNe (red) are compared with other types of SNe at most probable redshift ranges.